

---

# Phonon pseudoangular momentum in $\alpha$ -MoO<sub>3</sub>

Meiqi Li,<sup>1</sup> Zhibing Li,<sup>2,3,4</sup> Huanjun Chen,<sup>3,4,5</sup> and Weiliang Wang,<sup>1,4,6,a)</sup>

<sup>1</sup>School of Physics, Sun Yat-sen University, Guangzhou 510275, China

<sup>2</sup>School of Science, Shenzhen Campus of Sun Yat-sen University, Shenzhen 518107, China

<sup>3</sup>State Key Laboratory of Optoelectronic Materials and Technologies, Sun Yat-sen University, Guangzhou 510275, China

<sup>4</sup>Guangdong Province Key Laboratory of Display Material and Technology, Sun Yat-sen University, Guangzhou 510275, China

<sup>5</sup>School of Electronics and Information Technology, Sun Yat-sen University, Guangzhou 510275, China

<sup>6</sup>Center for Neutron Science and Technology, Sun Yat-sen University, Guangzhou 510275, China

<sup>a)</sup>Author to whom correspondence should be addressed: [wangwl2@mail.sysu.edu.cn](mailto:wangwl2@mail.sysu.edu.cn)

**Abstract:** In recent studies, it has been discovered that phonons can carry angular momentum, leading to a series of investigations into systems with 3-fold rotation symmetry. However, for systems with 2-fold screw rotational symmetry, such as  $\alpha$ -MoO<sub>3</sub>, there has been no relevant discussion. In this paper, we investigated the pseudoangular momentum of phonons in crystals with 2-fold screw rotational symmetry. Taking  $\alpha$ -MoO<sub>3</sub> as an example, we explain the selection rules in circularly polarized Raman experiments resulting from pseudoangular momentum conservation, providing important guidance for experiments. This study of pseudoangular momentum in  $\alpha$ -MoO<sub>3</sub> opens up a new degree of freedom for its potential applications, expanding into new application domains.

**Keywords:** phonon; pseudoangular momentum; selection rule; Helicity-selective Raman scattering;

## 1. Introduction

In recent years, pseudoangular momentum (PAM) as a novel degree of freedom for phonons has gained widespread attention. PAM is proposed as a quantized physical quantity defined by the eigenvalue of a rotation operator[1]. Phonon PAM exhibits selective coupling with other particles/quasiparticles, such as circularly polarized light[2,3], magnetization[4], phonon Berry curvature[5,6], and chiral structures[7], all of which are expected to lead to new physical effects. Therefore, in recent years, phonon PAM has aroused great interest. Both theory and experiment have revealed their significant contributions to various optical and excitonic effects in two-dimensional (2D) semiconductors[8,9], magneto-optical responses in topological semimetals[10], valley-phonon Hall effects[11], etc.

In first-order Raman scattering, recent studies have revealed robust selection rules for circularly polarized Raman experiments on 2D transition metal dichalcogenides (TMDs) with 3-fold rotational symmetry[3,12]. Zhang et al. [2] and Kyosuke Ishito et al.[13] found that the PAM in systems with 3-fold rotational symmetry, along with the angular momentum (AM) of photons, satisfies AM conservation in circularly polarized Raman scattering.

PAM has been systematically studied in systems with 3-fold rotational symmetry. However, for systems with 2-fold **screw** rotational symmetry (SRS), there has not yet been any relevant discussion.  $\alpha$ -MoO<sub>3</sub> is a system with 2-fold SRS. We take  $\alpha$ -MoO<sub>3</sub> as an example because of its in-plane anisotropy, making it a natural low-loss hyperbolic phonon polariton material[14,15]. It exhibits remarkable properties such as high spatial locality, slow group velocity[14], and tunability[16] of light, allowing for the compression and focusing of electromagnetic fields to very small scales[17,18]. Therefore, it has promising applications in integrated photonics chips. The discussion on its phonon PAM could open up a new tunable degree of freedom for its applications.

In 2021, Ali et al. carried out circularly polarized Raman experiments on  $\alpha$ -MoO<sub>3</sub>[19], but their analysis of the crystal orientation was wrong. Therefore, they failed to establish a connection between the selection rules in circularly polarized Raman experiments and the phonon PAM. Our study reveals that for  $\alpha$ -MoO<sub>3</sub>, there are no phonon modes with circular polarization at the  $\Gamma$  point. Therefore, to comprehend the selection rules in circularly polarized Raman spectroscopy, further investigation into the PAM of  $\alpha$ -MoO<sub>3</sub> is necessary.

In this work, we systematically discuss the PAM of the system with 2-fold SRS by group theory. Via revisiting the results of circularly polarized Raman experiments, we further elucidate the selection rules in circularly polarized Raman experiments of  $\alpha$ -MoO<sub>3</sub>. We find that it does not correlate with the expected chiral phonon

---

behavior (AM of phonon or so-called phonon circular polarization) but instead complies with conservation rules between phonon PAM and photon AM. The investigation of PAM in  $\alpha$ -MoO<sub>3</sub> provides a new degree of freedom for its related applications, opening a new application domain.

## 2. Methods

We performed first-principles calculations to study the phonon properties of  $\alpha$ -MoO<sub>3</sub>. The structure optimization, force constant calculations, and dielectric function calculations were conducted using density functional theory (DFT) implemented in the Vienna Ab initio Simulation Package (VASP).[20,21] The electron core interactions were assessed using the projector-augmented wave approximation[22]. The density function was estimated using the generalized gradient approximation with the Perdew–Burke–Ernzerhof (PBE)[23] exchange-correlation potential. The energy cutoff was set to 520. Because conventional DFT does not properly account for the vdW interaction, the lattice parameter perpendicular to the basal plane would be overestimated and a correction scheme is required to improve the results. Hence, optB88 is applied, which is a non-local van der Waals functional proposed by Berland and Cooper[24]. Harmonic approximation calculations of phonon frequencies and vibration vectors were obtained using the finite difference method implemented in Phonopy and VASP. The method of nonanalytical term correction (NAC)[25] was applied.

## 3. Results

### 3.1. PAM of phonon in lattices with 2-fold screw rotational symmetry

Displacement of the  $k$ -th atom in the  $l$ -th unit cell can be written as:

$$u_{\alpha} \left( \begin{smallmatrix} l \\ k \end{smallmatrix} \right) = \frac{1}{\sqrt{m_k N}} \sum_{j, \rho} \sum_{\mathbf{q}} e^{i\mathbf{q} \cdot \mathbf{R}_l} e_{\alpha} \left( k \middle| \begin{smallmatrix} \mathbf{q} \\ j, \rho \end{smallmatrix} \right) Q \left( \begin{smallmatrix} \mathbf{q} \\ j, \rho \end{smallmatrix} \right) \quad (1)$$

where  $Q \left( \begin{smallmatrix} \mathbf{q} \\ j, \rho \end{smallmatrix} \right) = Q_0 \left( \begin{smallmatrix} \mathbf{q} \\ j, \rho \end{smallmatrix} \right) e^{\pm i\omega(\mathbf{q}|j)t}$  is the amplitude of the  $j$ -th phonon mode,  $\rho$  is the index of degeneration,  $e_{\alpha} \left( k \middle| \begin{smallmatrix} \mathbf{q} \\ j, \rho \end{smallmatrix} \right)$  is the element of the eigenvector of the dynamical matrix,  $\alpha$  denotes the Cartesian index,  $\mathbf{q}$  is wave vector, and  $\mathbf{R}_l$  is the coordinates of atoms in real space.

Each phonon mode belongs to one of the irreducible representations (IR) of the space group at  $\mathbf{q}$ . The little group determines the symmetry of the harmonic potential term of phonons, so the symmetry of the eigenfunction must be described by the little group. A little group is a group composed of all operations within the crystallographic space group that remain reciprocal lattice invariant. A symmetry operation can be written as  $\hat{P} = \{\hat{R}|\hat{t}\}$ , where  $\hat{R}$  and  $\hat{t}$  are the rotation and translation parts, respectively. The translation vector  $\mathbf{t}$  can be further described as  $\mathbf{t} = \mathbf{T} + \boldsymbol{\tau}$ , where  $\boldsymbol{\tau}$  is a vector which is smaller than any primitive translation vector of the crystal, and  $\mathbf{T}$  is a translation vector of the crystal.

In symmorphic space groups with 2-fold rotation symmetry, The PAM was in terms of the eigenvalue of  $C_2$  acting on the phonon mode. Explicitly, we have

$$\{\widehat{C}_{2\alpha}|0\} \mathbf{u} \left( \begin{smallmatrix} l \\ k \end{smallmatrix} \right) = \exp[i\pi l_{\alpha}^{ph}] \mathbf{u} \left( \begin{smallmatrix} l \\ k \end{smallmatrix} \right) \quad (2)$$

where  $\alpha$  is the direction of the rotation axis. The phase correlation of the phonon wave function contains two parts: one is from the local (intracell) part  $\mathbf{e} \left( \begin{smallmatrix} \mathbf{q} \\ j \end{smallmatrix} \right)$ , and another is from the nonlocal (intercell) part  $e^{i\mathbf{q} \cdot \mathbf{R}_l}$ . Therefore, one can extract spin PAM  $l_{\alpha}^s$  for the local part and orbital PAM  $l_{\alpha}^o$  for the nonlocal part through rotation. [2]

When considering a system with SRS, we should define the PAM of phonons as follows[26]

$$\hat{P}_{\{R|\mathbf{t}\}} \mathbf{u} \left( \begin{smallmatrix} l \\ k \end{smallmatrix} \right) = \exp[-i\pi(l_o + l_s)] \mathbf{u} \left( \begin{smallmatrix} l \\ k \end{smallmatrix} \right) \quad (3)$$

For a system with SRS, the non-integer translation operations cannot be ignored. Let's first focus on the spin PAM  $l_{\alpha}^s$ . According to group theory analysis, the effect of a space group operation  $\hat{P} = \{\hat{R}|\hat{t}\}$  applied to the eigenvector of the dynamical matrix is:[27]

$$\hat{P}_{\{R|t\}} e_{\alpha} \left( k \left| \begin{smallmatrix} \mathbf{q} \\ j_{\rho} \end{smallmatrix} \right. \right) = e_{\alpha} \left( k' \left| \begin{smallmatrix} \mathbf{q} \\ j_{\rho} \end{smallmatrix} \right. \right) = \sum_k R e_{\alpha} \left( k \left| \begin{smallmatrix} \mathbf{q} \\ j_{\rho} \end{smallmatrix} \right. \right) e^{i\mathbf{q} \cdot (\mathbf{P}^{-1} \mathbf{R}_{0k'} - \mathbf{R}_{0k})} \delta_{Pk, k'} \quad (4)$$

where  $\delta_{Pk, k'}$  means that the atom  $k$  is transformed to atom  $k'$  by  $\hat{P}$ . For a little group operation  $\hat{P}^{\mathbf{q}} = \{\hat{R}_q | \hat{t}_q\}$ , that satisfies  $\mathbf{q} = R_q \mathbf{q} + \mathbf{G}$ , the element of IR is calculated by[28]

$$F_{j_{\rho} j'_{\rho}}(P_q) = \sum_{kk', \alpha, \beta} e_{\alpha}^* \left( k' \left| \begin{smallmatrix} \mathbf{q} \\ j_{\rho} \end{smallmatrix} \right. \right) R_q^{\alpha\beta} e_{\beta} \left( k \left| \begin{smallmatrix} \mathbf{q} \\ j'_{\rho} \end{smallmatrix} \right. \right) \times e^{i\mathbf{q} \cdot (\mathbf{P}_q^{-1} \mathbf{R}_{0k'} - \mathbf{R}_{0k})} \delta_{P_q k, k'} \quad (5)$$

where  $R_q^{\alpha\beta}$  represents the matrix elements of  $R_q$ . When the phonon mode is  $J$ -fold degenerate, IR is a  $J \times J$  matrix. The subscript  $j_{\rho}$  is the index for the rows and columns of the IR matrix. When  $J > 1$ , it is worth mentioning that the IR  $F(P_q)$  calculated by the first principle is usually not diagonalized. Thus, we need to transform the eigenvector to diagonalize  $F(P_q)$  before calculating  $l^s$ . After diagonalization, the  $j_{\rho}$ -th diagonal element  $F'_{j_{\rho}}(P_q)$  is the eigenvalue of the  $j_{\rho}$ -th degenerate phonon mode of the symmetry operations of  $\hat{P}^{\mathbf{q}} = \{\hat{R}_q | \hat{t}_q\}$ .

The spin PAM  $l_{\alpha}^s$  describes the rotation motion along the  $\alpha$ -axis. Therefore,  $l_{\alpha}^s$  is only related to atomic vibrations in the plane perpendicular to  $\alpha$  direction. Thus, when the non-integer translation operation  $\tau$  in  $P$  has a non-zero component only in the direction of  $\alpha$ , (e.g.  $\hat{P} = \{\hat{C}_{2y} | (0 \ \frac{1}{2} \ 0)\}$ ), the components of  $\mathbf{e} \left( \begin{smallmatrix} \mathbf{q} \\ j \end{smallmatrix} \right)$  that are perpendicular to  $\alpha$  direction can return to the original eigenstate (with an additional phase factor) after the rotational operation acting on it. Thus, the eigenvalue corresponding to the rotation operation can be obtained in this situation. Hence, only in this situation,  $l_{\alpha}^s$  can still be defined:[13]:

$$\{\hat{C}_{2\alpha} | 0\} e_{\beta\gamma} \left( \begin{smallmatrix} \mathbf{q} \\ j \end{smallmatrix} \right) = e^{in l_{\alpha}^s} e_{\beta\gamma} \left( \begin{smallmatrix} \mathbf{q} \\ j \end{smallmatrix} \right) \quad (6)$$

As  $F'_{j_{\rho}}(P_q)$  is an eigenvalue of the entire  $\hat{P}_{\{R|\tau\}}$ , hence we can obtain  $l_{\alpha}^s$  after eliminating the phase factor of the non-integer translation operation  $\hat{t}$ . We first need to obtain the eigenvalues of  $\hat{t}$  acting on the eigenvectors. Assuming  $\hat{t}^n = \hat{T}$ , where  $\hat{T}$  is an integer translation term. Therefore[26]:

$$\hat{t} e \left( \begin{smallmatrix} \mathbf{q} \\ j \end{smallmatrix} \right) = \hat{T}^{\frac{1}{n}} e \left( \begin{smallmatrix} \mathbf{q} \\ j \end{smallmatrix} \right) = e^{i\mathbf{q} \cdot \frac{\mathbf{T}}{n}} e \left( \begin{smallmatrix} \mathbf{q} \\ j \end{smallmatrix} \right) = e^{i\mathbf{q} \cdot \tau} e \left( \begin{smallmatrix} \mathbf{q} \\ j \end{smallmatrix} \right) \quad (7)$$

Hence, we obtained the eigenvalues of  $\hat{t}$  acting on  $\mathbf{e} \left( \begin{smallmatrix} \mathbf{q} \\ j \end{smallmatrix} \right)$ . After eliminating the phase factor of the non-integer translation operation  $\hat{t}$  in the eigenvalue of  $\hat{P}_{\{R|\tau\}}$ , we can obtain the spin PAM  $l_{\alpha}^s$  of  $j_{\rho}$ -th phonon mode

$$l_{\alpha}^s = -\frac{1}{i\pi} \left( \ln \left( F'_{j_{\rho} j_{\rho}}(P_q) \right) - i\mathbf{q} \cdot \tau \right) \quad (8)$$

In addition,  $\hat{P}$  is applied to  $e^{i\mathbf{q} \cdot \mathbf{R}_l}$  as follows[26]:

$$\hat{P}_{\{C_2|\tau\}} e^{i\mathbf{q} \cdot \mathbf{R}_l} = e^{i\mathbf{q} \cdot (\mathbf{P}^{-1} \mathbf{R}_l)} = e^{i\mathbf{q} \cdot (\{C_2^{-1} | -C_2^{-1} \tau\} \mathbf{R}_l)} = e^{i\{C_2\} \mathbf{q} \cdot (\mathbf{R}_l - \tau) - i\mathbf{q} \cdot \mathbf{R}_l} e^{i\mathbf{q} \cdot \mathbf{R}_l} \quad (9)$$

Therefore, we can obtain the orbital PAM  $l_{\alpha}^o$

$$l_{\alpha}^o = -\frac{1}{\pi} \{ (\mathbf{q} - C_2 \mathbf{q}) \cdot \mathbf{R}_{0k'} - C_2 \mathbf{q} \cdot \tau \} \quad (10)$$

According to Eq. (3), the total PAM is:

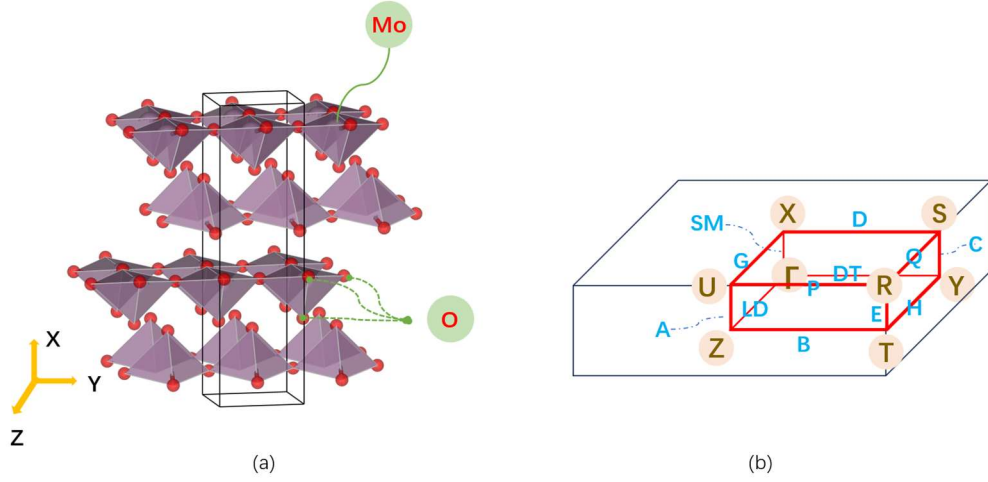
$$l_{\alpha}^{ph} = l_{\alpha}^o + l_{\alpha}^s \quad (11)$$

It is worth mentioning that this definition is only possible for nonsymmorphic systems with SRS whose non-integer translation operation  $\hat{t}$  in  $\hat{P}$  has a non-zero component only in the direction of  $\alpha$ .

### 3.2. PAM of phonon in $\alpha$ -MoO<sub>3</sub>

Based on this model, we calculate  $l_o$  and  $l_s$  for  $\alpha$ -MoO<sub>3</sub>.  $\alpha$ -MoO<sub>3</sub> is a typical material with a 2-fold SRS, belonging to the orthorhombic crystal system with space group Pnma (No.62). The crystal structure is illustrated in Figure. 1(a), in which crystallographic axes are shown, and Figure. 1(b) shows the First Brillouin zone.

**Figure 1.** (a) Atomic structure of  $\alpha$ -MoO<sub>3</sub>. The red balls represent oxygen atoms, forming the vertices of the pyramid, with a molybdenum atom at the center of the pyramid. The black solid lines indicate the unit cell. (b) First Brillouin zone of  $\alpha$ -MoO<sub>3</sub>[29].



At  $\Gamma$ , it is easy to calculate the PAM of  $\alpha$ -MoO<sub>3</sub>. We know  $l_{\alpha}^{ph} = l_{\alpha}^s$  since  $l_{\alpha}^o = 0$  when  $\mathbf{q} = 0$ , according to Eq. (10). At the meantime,  $F$  is a scalar since the phonon modes are non-degenerate at  $\Gamma$  point. Generally, lattice vibrational modes can be classified based on the IR of the space group. At the  $\Gamma$  point, there are four IRs with Raman activity, namely  $A_g$ ,  $B_{1g}$ ,  $B_{2g}$  and  $B_{3g}$ . We list in Table 1 the PAM values of phonon modes belonging to these four IRs at the  $\Gamma$  point, obtained with equation (8).

**Table 1.** PAM of  $\alpha$ -MoO<sub>3</sub> at  $\Gamma$  point

	$l_x^{ph}$	$l_y^{ph}$	$l_z^{ph}$
$A_g$	0	0	0
$B_{1g}$	1	1	0
$B_{2g}$	1	0	1
$B_{3g}$	0	1	1

Beyond  $\Gamma$ , the PAM of  $\alpha$ -MoO<sub>3</sub> depends on wave vector  $\mathbf{q}$ . For space group Pnma, there are three symmetry operations associated with rotation, and their matrix presentations are as follows

$$\{C_{2x}|\tau_x\} = \begin{pmatrix} 1 & 0 & 0 & \frac{1}{2} \\ 0 & -1 & 0 & \frac{1}{2} \\ 0 & 0 & -1 & \frac{1}{2} \end{pmatrix}, \quad (12)$$

$$\{C_{2y}|\tau_y\} = \begin{pmatrix} -1 & 0 & 0 & 0 \\ 0 & 1 & 0 & \frac{1}{2} \\ 0 & 0 & -1 & 0 \end{pmatrix}, \quad (13)$$

$$\{C_{2z}|\tau_z\} = \begin{pmatrix} -1 & 0 & 0 & \frac{1}{2} \\ 0 & -1 & 0 & 0 \\ 0 & 0 & 1 & \frac{1}{2} \end{pmatrix}, \quad (14)$$

The  $3 \times 3$  matrix on the left corresponds to the rotation operation  $C$ , and the last column corresponds to the non-integer translation operation  $\hat{t}$ . The three elements in the last column represent translations along the X/Y/Z direction, respectively. We can observe that in only Eq. (13), the non-integer translation terms are non-zero only in the direction of the rotation axis. Therefore, for Pnma, we can define  $l_{\alpha}^s$  only at those  $\mathbf{q}$ -points

whose corresponding little group possesses the  $\{\hat{C}_y|\hat{t}_y\}$  symmetry operation. In the first Brillouin zone, this condition is satisfied only for  $q$ -points at four high-symmetry paths parallel to  $\Gamma - Y$ (DT), i.e. the B, D, P and DT paths in Figure. 1(b). With group theory analysis, we can infer the characteristics of the phonon modes. On the DT path, the phonon mode degeneracy is 1, hence the IR is a scalar. The result of Eq. (5) turns out that the IR  $F(\{\hat{C}_y|\hat{t}_y\})$  has only two values, which are  $e^{i\pi q_y}$  and  $e^{i\pi(q_y+1)}$ , respectively. These also can be looked up from the IR table[30]. On the B path (Figure1.b), the phonon mode degeneracy is 2, thus the IR  $F(\{\hat{C}_y|\hat{t}_y\})$  are  $2 \times 2$  matrix. The result of Eq. (5) and the IR table[30] show that there is only one possible IR. In this case, the IR  $F(\{\hat{C}_y|\hat{t}_y\})$  is  $\begin{pmatrix} 0 & e^{i\pi q_y} \\ e^{i\pi q_y} & 0 \end{pmatrix}$ , whose eigenvalues are  $e^{i\pi q_y}$  and  $e^{i\pi(q_y+1)}$ . The results on the P and D paths are the same as those on the DT and B paths, respectively. To sum up, according to Eq. (8),  $l_y^s$  takes values of 0 and -1. According to Eq. (10),  $l_y^o$  is equal to  $q_y$ . Afterward, according to Eq. (11),  $l_y^{ph}$  takes values of  $q_y$  and  $q_y - 1$ , which is dependent on  $q$ . The values of phonon PAM along the DT high-symmetry path are shown in Figure. 2.

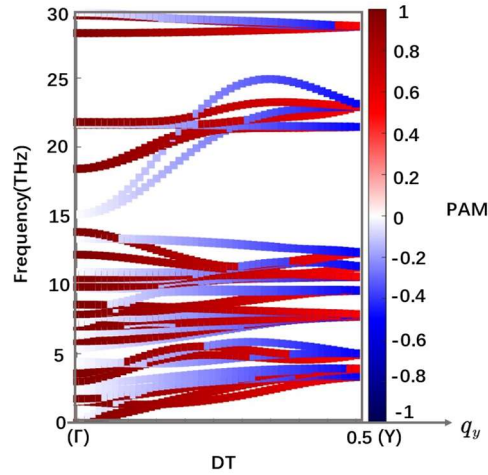


**Figure 2.** PAM of phonons along the  $\Gamma - Y$  (DT) high-symmetry path, ( $q_x=q_z=0$ ). The color axis represents PAM.

### 3.3. Helicity-selective Raman scattering

Raman scattering is a powerful tool for the structural identification and characterization of materials. Circularly polarized Raman spectroscopy, by measuring the frequency shift and rotation direction of photons interacting with molecular/crystal vibrations, reveals the symmetry, configuration, and rotational properties of molecules/crystals. This technique plays a significant role in fields such as materials science, biochemistry, and pharmaceutical research, aiding scientists in understanding the behavior and properties of molecules/crystals in the microscopic world.

In the work of Shahzad Akhtar Ali et al. [19], they report the observations of helicity selective Raman scattering from flakes of  $\alpha$ -MoO<sub>3</sub>. In their helicity-selective Raman scattering experiment, the flakes are oriented so that the crystallographic c- and a-axes align in-plane, and the incident light travels along the b-direction, which is perpendicular to the plane. In that study, the Raman tensors used are adapted from Ref.[31], in which the x-direction is the b-direction. Shahzad Akhtar Ali et al. erroneously used the y-direction as the direction of the incident wave vector in their theoretical analysis. As a result, deviations occurred in the theoretical analysis of the experimental results. Additionally, the authors failed to correlate the phonon's PAM with the experimental results of circularly polarized Raman scattering. Therefore, in our work, we reanalyzed the experimental results and provided a theoretical explanation of the intrinsic mechanism of this physical process.

The lattice parameters of  $\alpha$ -MoO<sub>3</sub> are  $a = 13.85 \text{ \AA}$ ,  $b = 3.71 \text{ \AA}$ , and  $c = 3.92 \text{ \AA}$ , with each primitive unit cell containing four Mo atoms and twelve O atoms. In this work, the layered structure of  $\alpha$ -MoO<sub>3</sub> was located in the b-c plane, designated as the y-z plane, as shown in Figure. 1(a).

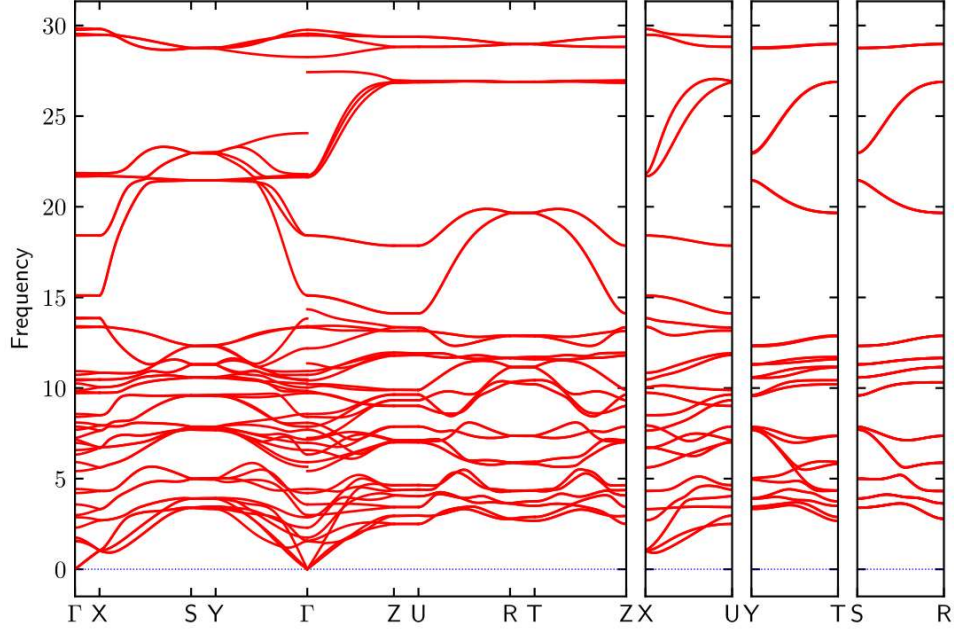


**Figure 3.** Phonon dispersion of  $\alpha - MoO_3$

From the phonon dispersion of  $\alpha$ - $MoO_3$  in Figure 3, we can see that there are no imaginary frequencies in the phonon dispersion.  $\alpha$ - $MoO_3$  has 45 optical phonon branches and 3 acoustic phonon branches. Group theory analysis reveals that the Raman-active modes are: 8  $A_g$ , 4  $B_{1g}$ , 8  $B_{2g}$ , and 4  $B_{3g}$ . According to group theory analysis, the Raman tensors of  $A_g$ ,  $B_{1g}$ ,  $B_{2g}$ ,  $B_{3g}$  should have the following form[31]

$$R(A_g) = \begin{pmatrix} a & 0 & 0 \\ 0 & b & 0 \\ 0 & 0 & c \end{pmatrix} \quad (15)$$

$$R(B_{1g}) = \begin{pmatrix} 0 & d & 0 \\ d & 0 & 0 \\ 0 & 0 & 0 \end{pmatrix} \quad (16)$$

$$R(B_{2g}) = \begin{pmatrix} 0 & 0 & e \\ 0 & 0 & 0 \\ e & 0 & 0 \end{pmatrix} \quad (17)$$

$$R(B_{3g}) = \begin{pmatrix} 0 & 0 & 0 \\ 0 & 0 & f \\ 0 & f & 0 \end{pmatrix} \quad (18)$$

It's worth noting that these Raman tensors apply to the XYZ convention illustrated in Figure. 1. The Raman scattering cross-section of a specific mode is proportional to  $|e_s^* \cdot R \cdot e_i|^2$ [32-37], where  $e_i$  and  $e_s$  denote the polarization direction of the incident laser and the scattered light.

First and foremost, it is crucial to note that, Shahzad Akhtar Ali et al. assert that the IR of the phonon mode with frequency of  $283 \text{ cm}^{-1}$  is  $B_{2g}$ . Nevertheless, based on our following reanalysis of the linearly polarized Raman experiment results on  $\alpha$ - $MoO_3$  and first-principles calculations results, we are inclined to assert that it should be  $B_{3g}$ . In the linearly polarized Raman experiments, the intensity varied as the sample rotated around the  $x$ -axis, which is the direction of the incident light wave vector. The intensity profiles were calculated as follows[31]

$$I_{A_g}(\theta) \propto \left| \begin{pmatrix} 0 \\ 1 \\ 0 \end{pmatrix}^T \begin{pmatrix} 1 & 0 & 0 \\ 0 & \cos\theta & -\sin\theta \\ 0 & \sin\theta & \cos\theta \end{pmatrix}^T R(A_g) \begin{pmatrix} 1 & 0 & 0 \\ 0 & \cos\theta & -\sin\theta \\ 0 & \sin\theta & \cos\theta \end{pmatrix} \begin{pmatrix} 0 \\ 1 \\ 0 \end{pmatrix} \right|^2 \quad (19)$$

$$= |b\cos^2\theta + c\sin^2\theta|^2$$

$$I_{B_{3g}}(\theta) \propto |f \sin 2\theta|^2 \quad (20)$$

$$I_{B_{2g}}(\theta) = I_{B_{1g}}(\theta) = 0 \quad (21)$$

where  $(0 \ 1 \ i)^T$  represents linearly polarized light with polarization direction along the y-axis. We can see that only the Raman intensity of the  $A_g$  and  $B_{3g}$  modes can be observable. This implies that the phonon mode with a frequency of  $283 \text{ cm}^{-1}$  is by no means as they analyzed, attributed to  $B_{2g}$ . Through first-principles calculations, we know that there is a phonon mode with an IR of  $B_{3g}$  whose frequency is close to the mentioned frequency. Therefore, we believe that the phonon mode with a frequency of  $283 \text{ cm}^{-1}$  has an IR of  $B_{3g}$ . In summary, in the circularly polarized Raman experiment, the authors should have detected Raman signals for three  $A_g$  modes (at  $336, 817, \text{ and } 992 \text{ cm}^{-1}$ ) and two  $B_{3g}$  modes (at  $283 \text{ and } 666 \text{ cm}^{-1}$ ). Furthermore, we analyze the experimental results of circularly polarized Raman spectroscopy. Firstly, we calculated the Raman scattering intensity of the circularly polarized. Circularly polarized light is divided into left-handed and right-handed categories, commonly described using helicity and also indicated by spin AM. When the wave vector direction is along the x-axis, left-circularly polarized light is represented as  $(0 \ 1 \ i)^T$ , with spin AM  $m_{\text{photon}} = -1$ , and right-circularly polarized light is represented as  $(0 \ 1 \ -i)^T$ , with spin AM  $m_{\text{photon}} = +1$ . Similar conventions apply to the other two directions. Our computational results are listed in Table 2. The column groups in the background color Yellow/Green/Red in Table 2 correspond to the light's AM along the X/Y/Z axis, with the propagation direction of both incident and scattered light also along the X/Y/Z axis. The double wavy underlines indicate modes with strong Raman intensity have been detected in the experiment [19]. The experimental results are consistent with our prediction of the Raman intensity.

**Table 2.** Raman intensity depending on the electric polarization.  $\checkmark$  represents that the Raman intensity can be nonzero, and  $\times$  indicates that the Raman intensity should be zero.

incident laser	(0 1 i)		(1 0 i)		(1 i 0)	
scattered light	$\begin{pmatrix} 0 \\ 1 \\ i \end{pmatrix}$	$\begin{pmatrix} 0 \\ 1 \\ -i \end{pmatrix}$	$\begin{pmatrix} 1 \\ 0 \\ i \end{pmatrix}$	$\begin{pmatrix} 1 \\ 0 \\ -i \end{pmatrix}$	$\begin{pmatrix} 1 \\ i \\ 0 \end{pmatrix}$	$\begin{pmatrix} 1 \\ -i \\ 0 \end{pmatrix}$
$A_g$	<u><math>\checkmark</math></u>	<u><math>\checkmark</math></u>	$\checkmark$	$\checkmark$	$\checkmark$	$\checkmark$
$B_{1g}$	$\times$	$\times$	$\times$	$\times$	$\checkmark$	$\checkmark$
$B_{2g}$	$\times$	$\times$	$\checkmark$	$\checkmark$	$\times$	$\times$
$B_{3g}$	$\times$	<u><math>\checkmark</math></u>	$\times$	$\times$	$\times$	$\times$

The behavior of circularly polarized light in Raman scattering can be predicted by the Raman tensor[32]. However, the classical theory cannot tell us the intrinsic mechanism. Thus, it is an important issue to study the PAM of phonons and the conservation law of the PAM of phonons[2,8] in a crystal.

In existing circularly polarized Raman experiments, samples are probed using circularly polarized light, and then the circular polarization of the scattered light is detected. For some modes of phonon, the helicity of the scattered light is opposite to that of the incident light, with  $\Delta m_{\text{photon}} = \pm 2$  ( $\checkmark$  in the second column in each colored group in Table 2). For some other modes of phonon, the helicity of the scattered light is the same as that of the incident light, with  $\Delta m_{\text{photon}} = 0$  ( $\checkmark$  in the first column in each colored group in Table 2). Since the incident light and the scattered light travelled along the x and the -x direction, respectively. It can be seen that only the Raman scattering intensity of the  $A_g$  and  $B_{3g}$  modes could be non-zero, because the PAM of these phonon modes along x direction is 0 ( $l_x^{\text{ph}} = 0$ ); the Raman scattering intensity of the  $B_{1g}$  and  $B_{2g}$  modes should be zero, because the PAM of these phonon modes along x direction is 1 ( $l_x^{\text{ph}} = 1$ ). A similar analysis

holds for the other two directions. Based on the computed Raman intensity (Table 2) and experimental results, we can infer: that as a selection rule for the optical transition process, PAM offers an additional conservation condition besides the crystal momentum conservation and energy conservation. Due to momentum matching requirements, we generally consider phonons at the  $\Gamma$ -point to couple with light in terms of AM, which follows the selection rule[38] in a crystal with 2-fold SRS

$$m_i - m_s = -l_\alpha^{ph} + 2p(p=0,\pm 1) \quad (22)$$

where  $m_s$  and  $m_i$  represent the AM of the scattered and incident photons, respectively. Thus, the selection rule can be described as follows: if the sum of photon AM and phonon PAM is not conserved, the Raman effect cannot occur. If the sum of photon AM and phonon PAM change is conserved, the Raman effect may occur.

#### 4. Conclusions

We systematically discuss the PAM in a crystal with 2-fold SRS. For  $\alpha$ -MoO<sub>3</sub>, PAM is only discussable along the high-symmetry path parallel to  $\Gamma - Y$ . We provide the PAM values on the  $\Gamma - Y$  path, which are associated with  $q$ -points, taking values of  $q_y$  and  $q_y - 1$ . Furthermore, due to momentum matching requirements, we generally consider phonons at the  $\Gamma$ -point to couple with light in terms of AM. We discussed the PAM values at the  $\Gamma$ -point and clarified the selection rules in circularly polarized Raman experiments of  $\alpha$ -MoO<sub>3</sub> through theoretical analysis and examination of experimental results. We discover that it doesn't conform to previous expectations related to chiral phonons but rather complies with conservation rules on the sum of phonon PAM and photon AM. For circularly polarized incident light and scattered light,  $\Delta m_{photo} = 2$  or  $\Delta m_{photo} = 0$ , only phonons with PAM=0 have non-zero Raman scattering intensity, while phonons with PAM=1 always have zero Raman scattering intensity. For  $\alpha$ -MoO<sub>3</sub>, when the AM of the incident light is along the out-of-plane-direction, only  $A_g$  and  $B_{3g}$  modes exhibit nonzero Raman scattering intensity. This investigation of PAM in  $\alpha$ -MoO<sub>3</sub> paves the way for its potential applications.

**Acknowledgments:** This work was supported by the National Natural Science Foundation of China (no. 91963205); the Science and Technology Planning Project of Guangdong Province (2023B1212060025) and the Physical Research Platform (PRP) in School of Physics, SYSU.



## References

1. Zhang, L.; Niu, Q. Angular Momentum of Phonons and the Einstein–de Haas Effect. *Physical Review Letters* **2014**, *112*, 085503, doi:10.1103/PhysRevLett.112.085503.
2. Zhang, L.; Niu, Q. Chiral phonons at high-symmetry points in monolayer hexagonal lattices. *Phys Rev Lett* **2015**, *115*, 115502, doi:10.1103/PhysRevLett.115.115502.
3. Chen, S.Y.; Zheng, C.; Fuhrer, M.S.; Yan, J. Helicity-resolved Raman scattering of MoS(2), MoSe(2), WS(2), and WSe(2) atomic layers. *Nano Lett* **2015**, *15*, 2526–2532, doi:10.1021/acs.nanolett.5b00092.
4. Hamada, M.; Minamitani, E.; Hirayama, M.; Murakami, S. Phonon Angular Momentum Induced by the Temperature Gradient. *Physical Review Letters* **2018**, *121*, 175301, doi:10.1103/PhysRevLett.121.175301.
5. Zhang, L.; Ren, J.; Wang, J.-S.; Li, B. Topological Nature of the Phonon Hall Effect. *Physical Review Letters* **2010**, *105*, 225901, doi:10.1103/PhysRevLett.105.225901.
6. Liu, Y.; Xu, Y.; Duan, W. Berry phase and topological effects of phonons. *National Science Review* **2018**, *5*, 314–316, doi:10.1093/nsr/nwx086.
7. Chen, H.; Wu, W.; Zhu, J.; Yang, Z.; Gong, W.; Gao, W.; Yang, S.A.; Zhang, L. Chiral Phonon Diode Effect in Chiral Crystals. *Nano Letters* **2022**, *22*, 1688–1693, doi:10.1021/acs.nanolett.1c04705.
8. Hanyu Zhu; Jun Yi; Ming-Yang Li; Jun Xiao; Lifa Zhang; Chih-Wen Yang; Robert A. Kaindl; Lain-Jong Li; Yuan Wang; Zhang, X. Observation of chiral phonons. *Science* **2018**, 579–582
9. Chen, H.; Zhang, W.; Niu, Q.; Zhang, L. Chiral phonons in two-dimensional materials. *2D Materials* **2019**, *6*, 012002, doi:10.1088/2053-1583/aaf292.
10. Mankowsky, R.; Först, M.; Cavalleri, A. Non-equilibrium control of complex solids by nonlinear phononics. *Reports on Progress in Physics* **2016**, *79*, 064503, doi:10.1088/0034-4885/79/6/064503.
11. He, M.; Rivera, P.; Van Tuan, D.; Wilson, N.P.; Yang, M.; Taniguchi, T.; Watanabe, K.; Yan, J.; Mandrus, D.G.; Yu, H.; et al. Valley phonons and exciton complexes in a monolayer semiconductor. *Nature Communications* **2020**, *11*, 618, doi:10.1038/s41467-020-14472-0.
12. Zhao, Y.; Han, S.; Zhang, J.; Tong, L. Helicity-resolved resonant Raman spectroscopy of layered WS<sub>2</sub>. *Journal of Raman Spectroscopy* **2021**, *52*, 525–531, doi:10.1002/jrs.5996.
13. Ishito, K.; Mao, H.; Kousaka, Y.; Togawa, Y.; Iwasaki, S.; Zhang, T.; Murakami, S.; Kishine, J.-i.; Satoh, T. Truly chiral phonons in  $\alpha$ -HgS. *Nature Physics* **2022**, *19*, 35–39, doi:10.1038/s41567-022-01790-x.
14. Nano, I.o.F.; Soft Materials, J.K.L.f.C.-b.F.M.; Devices; Science, C.I.C.o.S.N.; Technology, S.U., Suzhou, China.; Departamento de Física, U.d.O., Oviedo, Spain. pabloalonso@uniovi.es.; Nano, I.o.F.; Soft Materials, J.K.L.f.C.-b.F.M.; Devices; Science, C.I.C.o.S.N.; et al. In-plane anisotropic and ultra-low-loss polaritons in a natural van der Waals crystal. *Nature* **2018**, *562*, 557–562.
15. Zebo, Z.; Ningsheng, X.; L, O.S.; Michele, T.; Fengsheng, S.; Yinzhu, J.; Yanlin, K.; Jianing, C.; Wuchao, H.; L, W.W.; et al. A mid-infrared biaxial hyperbolic van der Waals crystal. *Science Advances* **2019**, *5*, eaav8690.
16. Zheng, Z.; Chen, J.; Wang, Y.; Wang, X.; Chen, X.; Liu, P.; Xu, J.; Xie, W.; Chen, H.; Deng, S.; et al. Highly Confined and Tunable Hyperbolic Phonon Polaritons in Van Der Waals Semiconducting Transition Metal Oxides. *Advanced Materials* **2018**, *30*, 1705318, doi:10.1002/adma.201705318.
17. Javier, M.; Jiahua, D.; Javier, T.; Gonzalo, Á.; V, V.K.; Iván, P.; Weiliang, M.; Qiaoliang, B.; S, V.V.; Rainer, H.; et al. Focusing of in-plane hyperbolic polaritons in van der Waals crystals with tailored infrared nanoantennas. *Science advances* **2021**, *7*, eabj0127.
18. Folland, T.G.; Caldwell, J.D. Precise control of infrared polarization using crystal vibrations. *Nature* **2018**, *562*, 499–501, doi:10.1038/d41586-018-07087-5.

19. Ali, S.A.; Irfan, A.; Mazumder, A.; Balendhran, S.; Ahmed, T.; Walia, S.; Ulhaq, A. Helicity-selective Raman scattering from in-plane anisotropic  $\alpha$ -MoO<sub>3</sub>. *Applied Physics Letters* **2021**, *119*, 193104, doi:10.1063/5.0064464.
20. G. Kresse et al.; J.F. Efficiency of ab-initio total energy calculations for metals and semiconductors using a plane-wave basis set. *Computational Materials Science* **1996**, 15-50.
21. Vanderbilt, D. Soft self-consistent pseudopotentials in a generalized eigenvalue formalism. *Phys Rev B Condens Matter* **1990**, *41*, 7892-7895, doi:10.1103/physrevb.41.7892.
22. Kresse, G.; Joubert, D. From ultrasoft pseudopotentials to the projector augmented-wave method. *PHYSICAL REVIEW B* **1999**, 1758.
23. John P. Perdew; Kieron Burke; Ernzerhof, M. Generalized Gradient Approximation Made Simple. *PHYSICAL REVIEW LETTERS* **1996**, 3865.
24. Klimes, J.; Bowler, D.R.; Michaelides, A. Chemical accuracy for the van der Waals density functional. *J Phys Condens Matter* **2010**, *22*, 022201, doi:10.1088/0953-8984/22/2/022201.
25. Gonze, X.; Lee, C. Dynamical matrices, Born effective charges, dielectric permittivity tensors, and interatomic force constants from density-functional perturbation theory. *Physical Review B* **1997**, *55*, 10355-10368, doi:10.1103/PhysRevB.55.10355.
26. Zhang, T.; Murakami, S. Chiral phonons and pseudoangular momentum in nonsymmorphic systems. *Physical Review Research* **2022**, *4*, L012024, doi:10.1103/PhysRevResearch.4.L012024.
27. Maradudin, A.A.; Vosko, S.H. Symmetry Properties of the Normal Vibrations of a Crystal. *Reviews of Modern Physics* **1968**, *40*, 1-37, doi:10.1103/RevModPhys.40.1.
28. Togo, A. First-principles Phonon Calculations with Phonopy and Phono3py. *Journal of the Physical Society of Japan* **2023**, *92*, 012001, doi:10.7566/jpsj.92.012001.
29. Setyawan, W.; Curtarolo, S. High-throughput electronic band structure calculations: Challenges and tools. *Computational Materials Science* **2010**, *49*, 299-312, doi:10.1016/j.commatsci.2010.05.010.
30. Elcoro, L.; Bradlyn, B.; Wang, Z.; Vergniory, M.G.; Cano, J.; Felser, C.; Bernevig, B.A.; Orobengoa, D.; de la Flor, G.; Aroyo, M.I. Double crystallographic groups and their representations on the Bilbao Crystallographic Server. *Journal of Applied Crystallography* **2017**, *50*, 1457-1477, doi:<https://doi.org/10.1107/S1600576717011712>.
31. Wen, M.; Chen, X.; Zheng, Z.; Deng, S.; Li, Z.; Wang, W.; Chen, H. In-Plane Anisotropic Raman Spectroscopy of van der Waals  $\alpha$ -MoO<sub>3</sub>. *The Journal of Physical Chemistry C* **2020**, *125*, 765-773, doi:10.1021/acs.jpcc.0c09178.
32. Loudon, R. The Raman effect in crystals. *Advances in Physics* **1964**, *13*, 423-482, doi:10.1080/00018736400101051.
33. Kranert, C.; Sturm, C.; Schmidt-Grund, R.; Grundmann, M. Raman tensor elements of  $\beta$ -Ga<sub>2</sub>O<sub>3</sub>. *Scientific Reports* **2016**, *6*, 35964, doi:10.1038/srep35964.
34. Ding, Y.; Zheng, W.; Lin, Z.; Zhu, R.; Jin, M.; Zhu, Y.; Huang, F. Raman tensor of layered WS<sub>2</sub>. *Science China Materials* **2020**, *63*, 1848-1854, doi:10.1007/s40843-020-1321-4.
35. Pimenta, M.A.; Resende, G.C.; Ribeiro, H.B.; Carvalho, B.R. Polarized Raman spectroscopy in low-symmetry 2D materials: angle-resolved experiments and complex number tensor elements. *Phys. Chem. Chem. Phys.* **2021**, *23*, 27103-27123, doi:10.1039/D1CP03626B.
36. Jin, M.; Cheng, L.; Zheng, W.; Ding, Y.; Zhu, Y.; Jia, L.; Huang, F. Raman tensor of graphite: Symmetry of G, D and D' phonons. *Science China Materials* **2022**, *65*, 268-272, doi:10.1007/s40843-021-1741-0.
37. Liu, S.; Long, M.-Q.; Wang, Y.-P. Theoretical investigations on the magneto-Raman effect of CrI<sub>3</sub>. *Physical Review B* **2023**, *108*, 184414, doi:10.1103/PhysRevB.108.184414.
38. Tatsumi, Y.; Kaneko, T.; Saito, R. Conservation law of angular momentum in helicity-dependent Raman and

Rayleigh scattering. *Physical Review B* **2018**, *97*, 195444, doi:10.1103/PhysRevB.97.195444.